Application of a spore detection system based on diffraction imaging to tomato gray mold

Yafei Wang[1,2], Qiang Shi[3], Shanjian Ren[1], Tiezhu Li[1], Ning Yang[4], Xiaodong Zhang[1], Guoxin Ma[1], Mohamed Farag Taha[1,5], Hanping Mao[1*]

(1. *School of Agricultural Engineering, Jiangsu University, Zhenjiang 212013, Jiangsu, China*;
2. *Jiangsu Changdian Technology Co. Ltd, Jiangyin 214400, Jiangsu, China*;
3. *School of Science and Technology, Shanghai Open University, Shanghai 200433, China*;
4. *School of Electrical and Information Engineering, Jiangsu University, Zhenjiang 212013, Jiangsu, China*;
5. *Department of Soil and Water Sciences, Faculty of Environmental Agricultural Sciences, Arish University, North Sinai, 45516, Egypt*)

Abstract: This study addresses the challenge posed by the small spore size of tomato gray mold, which hinders its identification and enumeration by conventional techniques. This work presents a novel approach for quantifying spore counts of tomato gray mold using diffraction imaging technology and image processing techniques. To construct a device for acquiring diffraction images of tomato gray mold spores, initially, the hyperspectral data pertaining to the gray mold spores of tomatoes was obtained. The characteristic wavelength of the light source of the diffraction image acquisition device was obtained by smoothing, principal component analysis, and comprehensive coefficient weight calculation. Then, the key parameters of the system were simulated, and the diffraction image acquisition device was built. Finally, tomato gray mold spores were counted based on angular spectrum reconstruction and image processing. The findings indicated that the combined contribution rate of the initial and secondary principal components of the original spectral data obtained from tomato gray mold spore samples amounted to 92.271%. The visible range of 435 nm, 475 nm, and 720 nm can be selected as the light source for tomato gray mold's spore diffraction imaging system. CMOS image sensor was installed 45 mm below the micropore with a diameter of 100 μm, and the diffraction image obtained by simulation has a clear diffraction fingerprint. The diffraction imaging system can collect diffraction images of disease spores, and the collected diffraction images have clear diffraction fingerprints. The experimental error range was 5.13%-8.57%, and the average error was 6.42%. The error was within a 95% consistency. Therefore, this study can provide a research basis for the classification and recognition of greenhouse disease spores.

Keywords: greenhouse, tomato gray mold, spore detection, diffraction imaging, image processing
DOI: 10.25165/j.ijabe.20241706.8537

Citation: Wang Y F, Shi Q, Ren S J, Li T Z, Yang N, Zhang X D, et al. Application of a spore detection system based on diffraction imaging to tomato gray mold. Int J Agric & Biol Eng, 2024; 17(6): 212–217.

1 Introduction

Tomatoes are one of the most widely consumed vegetables in the world due to their being a staple vegetable in most meals and their great nutritional value[1,2]. At present, China has become the largest producer and consumer of tomatoes in the world, with a planting area of 1.01 million hm^2[3,4]. Tomato gray mold is a worldwide disease affecting many plants[5]. Botrytis cinerea, the fungus responsible for tomato gray mold disease, can invade the root, stem, and leaf[6,7]. Generally, the yield of tomatoes will drop by 20%-30% after the occurrence of gray mold, and it can be as high as 50% in serious cases[8]. In addition, pathogenic fungi can infect tomato fruits through skin damage during harvesting and processing, which leads to rapid deterioration, considerable economic losses, and short shelf life[6,9]. Therefore, it is of great significance to monitor tomato gray mold in time and take effective preventive measures to ensure tomato yield and improve farmers' economic income.

With the development of computer technology and spore catcher technology, related researchers have employed spore capture instruments to collect disease spores from the air, then count and identify the spores using microscopic image processing[10,11]. However, conventional microscopic imaging technology encounters limitations regarding its restricted field of view, making obtaining a comprehensive image of spores challenging and leading to significant inaccuracies[12,13]. In recent years, holographic imaging technology has been favored by related researchers because of its small size and portability. Luo et al.[14] combined lensless microscopy with deep learning to measure the target analyte for quantitative particle agglutination test. Xiao et al.[15] used digital holographic microscopy to study the delayed morphogenesis of

Received date: 2023-09-15 **Accepted date:** 2024-06-04
Biographies: Yafei Wang, PhD, Lecturer, research interest: intelligent agricultural equipment and technology, Email: wangyafei918@126.com; **Qiang Shi**, PhD, Associate Professor, research interest: intelligent agricultural equipment and technology, Email: openagriculture@163.com.; **Shanjian Ren**, Undergraduate, research interest: mechanical design and automation, Email: 209551973@qq.com.; **Tiezhu Li**, MS candidate, research interest: intelligent agricultural equipment and technology, Email: 2212316059@stmail.ujs.edu.cn; **Ning Yang**, PhD, Professor, research interest: intelligent agricultural equipment and technology, Email: yangning7410@163.com; **Xiaodong Zhang**, PhD, Professor, research interest: intelligent agricultural equipment and technology, Email: zxd700227@126.com; **Guoxin Ma**, PhD, Lecturer, research interest: intelligent agricultural equipment and technology, Email: mgx@ujs.edu.cn; **Mohamed Farag Taha**, Postdoctoral, research interest: intelligent agricultural equipment and technology, Email: 1000006483@ujs.edu.cn
***Corresponding author: Hanping Mao**, PhD, Professor, research interest: modern agricultural equipment and the environmental control technology of facility agriculture. Department of agricultural equipment, Jiangsu University, Zhenjiang 212013, Jiangsu, China. Email: maohpujs@163.com.

living bone cells. Prajapati et al.[16] reported a micro-lensless microscope on a chip and used it to image human blood smears and microbeads up to 1 μm in diameter. The disease spores and the objects studied by these scholars are μm level, so we can learn from the previous research results and apply holographic imaging technology to detect disease spores. Xin et al.[17] used digital holographic flow cytometry to rapidly capture images of diverse cell types present in urine and to reconstruct high-precision quantitative phase images for each cell type. Natalith et al.[18] processed hologram height variations, shape, and length of KA cells, as well as the stratum corneum epidermal layer, which are obtained as phase images. The results aided in discriminating healthy from malignant cells. The diffraction image method can be used to screen particles with small particle sizes[19]. However, the size, shape, protein, and nucleic acid of tomato gray mold spores are different from other cells. Their findings cannot be directly applied to the detection of tomato gray mold spores. The specific absorption spectrum information and diffraction imaging distance of tomato gray mold spores need to be studied.

Therefore, this study aimed to develop an imaging apparatus utilizing diffraction imaging technology to capture diffraction images of tomato gray mold spores within a greenhouse environment. A method based on diffraction reconstruction was proposed to count the spores of gray mold. Finally, the spore count of tomato gray mold was realized.

2 System structure

The two-dimensional structure diagram of the spore diffraction image acquisition device for tomato gray mold is shown in Figure 1. The diffraction image acquisition device mainly includes a light source, micro-hole, slide, and CMOS image sensor. The micro-hole was located directly below the light source, which was used to generate interference light. Tomato gray mold spores were collected on the slide. The diffraction image of spores was collected with a CMOS image sensor, which was connected to the computer via a data cable. The computer was equipped with the diffraction fingerprint image acquisition software Arena View-Arena View2.

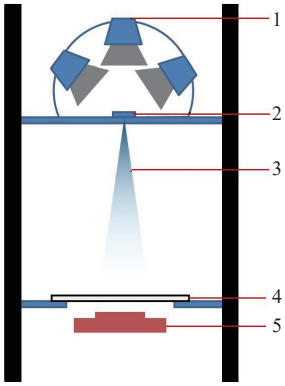

1. Light source 2. Micro-hole 3. Interference light 4. Slide 5. CMOS image sensor

Figure 1 Structure diagram of diffraction imaging device

3 Band selection

3.1 Sample preparation

The cultivation experiment of tomato plant samples was carried out in Venlo Greenhouse, Jiangsu University. The tested tomato variety was “Zhefen 202” (Zhejiang Yinong Seed Industry Co., Ltd., China). It is not advisable to apply pesticide sprays during the process of planting samples. In vitro cultivation of tomato gray mold spores is feasible. To acquire a pristine sample of spores from tomato gray mold, it is necessary to ensure the absence of any contamination. When gray mold occurred in tomato plants during the experiment, leaves with diseased spots were first cut from infected plants. After dipping in sterile water, the spot was placed face down on a non-diseased tomato plant. This was repeated until gray mold was the only spot on the tomato plant. Then, the tomato leaves with gray mold were placed in a petri dish with a Potato Dextrose Agar (PDA) medium for culture preservation and propagation.

3.2 Spectral data acquisition

The spectrum data of tomato gray mold spores was acquired using a hyperspectral imaging system. The system includes a hyperspectral image camera (ImSpector, V10E, Spectra Imaging Ltd., Finland), a light source system (2900, Illumination Technologies Inc., USA), displacement console (Zolix TS200AB, Zolix Hanguang, China), camera obscura (DC1300, Wuling Optics, China), data acquisition and preprocessing software (SpectraCube, Auto Vision Inc., USA), and computers. Before use, the instrument was preheated for 30 min, and then the black-and-white version was corrected. During the actual collection process, the petri dish samples with spore colonies of tomato gray mold were placed on the displacement console. The camera exposure time was set to 50 ms. The moving speed of the displacement table was 1.25 mm/s. The image resolution of the hyperspectral camera was 819 pixels× 1024 pixels. The spectral resolution was 2.8 nm. The spectral range was 400-1000 nm. The original spectral data of tomato gray mold spores collected are shown in Figure 2.

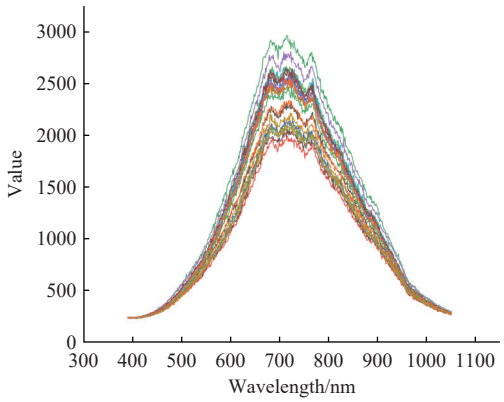

Figure 2 Original spectral data of spores

3.3 Feature band selection

The raw spectrum data obtained from the hyperspectral imaging equipment for tomato gray mold spores was expected to include certain levels of noise. Hence, it is imperative to perform preprocessing on the spectral data obtained from samples. To eliminate the influence of noise on the original spectral analysis, S-G (Savitzky-Golay) five-point smoothing was used in this study to process the original spectral data of tomato gray mold spores[20]. The smoothed spectral data is shown in Figure 3.

Many bands exist in the original spectral data of tomato gray mold spore samples. Also, there is a lot of information redundancy between bands. Therefore, reducing the dimensionality of the original spectral data is necessary. Selecting an appropriate data dimensionality reduction algorithm can improve the modeling efficiency and accuracy of spectral data[21]. In this study, principal component analysis (PCA) was used to select the characteristic wavelength of the original spectral data of tomato gray mold spore samples, to reduce the dimension of the original spectral data. After

smoothing the spectral data of tomato gray mold spore samples, they were analyzed by SPSS 22 software, and 17 principal components were obtained. The cumulative contribution rates of the first principal component and the second principal component are listed in Table 1.

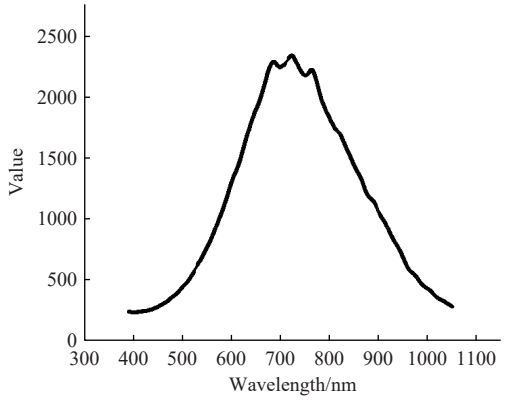

Figure 3 Spectral data of spore samples after smoothing processing

Table 1 PCA principal component accumulation contribution rate

Principal component	PC1	PC2
Cumulative contribution rate/%	89.072	92.271

Local peaks and valleys of the spectrum were identified to highlight the significantly affected wavelengths of the tomato gray mold spore sample by principal component analysis protocol. This is because the wavelengths located at the local maximums (peaks) or minimums (valleys) of the loading curve have the greatest contribution to the PC loadings. Two PCs were selected with a cumulative contribution of 92.271% of the variance. The linear combination coefficient, variance, and composite score model coefficient of the first principal component and the second principal component were solved, respectively. Finally, the combined coefficient weights of the first and second principal components were obtained, as shown in Figure 4.

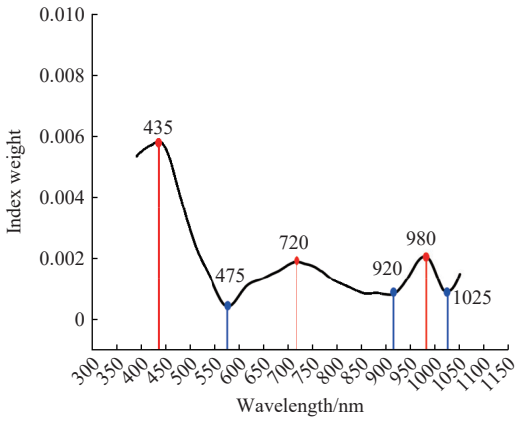

Figure 4 Comprehensive coefficient weights of principal components

As shown in Figure 4, the combined coefficient weights of the first and second principal components of the spectral data of tomato gray mold spore samples have three peaks in the band range 390-1050 nm, corresponding to the bands 435 nm, 722 nm, and 980 nm, respectively. The original spectral data of tomato gray mold spore samples in the visible light range and the combination coefficient weights of the first and the second principal components were considered. In this study, the light sources of 435 nm, 475 nm, and 720 nm were selected as the light sources for the diffraction imaging system of tomato gray mold spores.

4 Key parameter design

4.1 Light source design

Based on the previous analysis, this study selected LED lamp beads with wavelengths of 435 nm, 475 nm, and 720 nm as light sources. However, as a diffraction imaging system, the light source also needs a power supply circuit and a circuit to adjust the brightness of the light source. Therefore, this study uses Altium Designer software to draw the circuit diagram of the light source and import it into the PCB diagram. Then, the PCB circuit board is made, and finally, it is welded into a light source. The light source part was used to emit light at wavelengths of 435 nm, 475 nm, and 720 nm with stable light intensity. The angle between the light source and the center of the receiving part of the three bands was 120°. The light source circuit of the diffraction imaging system and the physical diagram of the light source are shown in Figure 5.

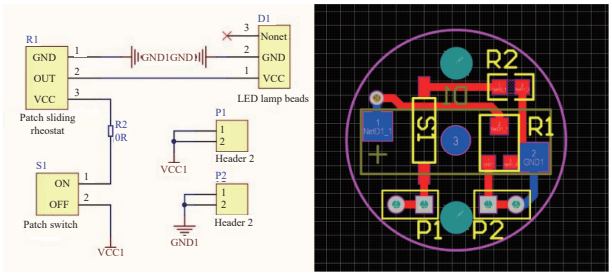

a. Schematic diagram b. PCB diagram

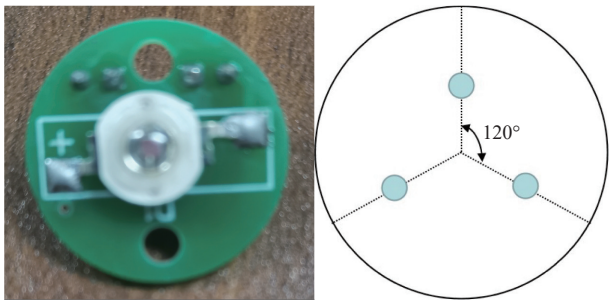

c. Light source d. Light source arrangement

Figure 5 Diffraction imaging light source design

4.2 CMOS image sensor selection

The diffraction imaging system of this study was designed to capture data on tomato gray mold spores in greenhouses. Considering the actual situation, the disease spores collected in the greenhouse are generally more than ten to dozens every day. Suppose the disease spores were collected for a month. The compound field microfluidic chip developed by the research group of this study was used to enrich the spores, and the enrichment area was 1000 μm in radius[22]. In addition, the summer greenhouse temperature can reach 50°C in a short time. To meet the above conditions, the CMOS image sensor of the DYSMT805 model was selected to collect the spore's diffraction image. The spectral response range of the CMOS image sensor is 310-1070 nm. The sensitive size is 4592 μm×3449.6 μm. The pixel size is 1.4 μm× 1.4 μm. The operating temperature is 0°C-50°C, and storage temperature is −30°C-70°C. It can meet the requirements of practical applications. The actual picture of the selected CMOS image sensor is shown in Figure 6.

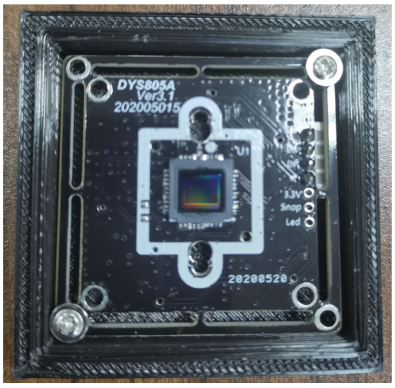

Figure 6 CMOS image sensor of DYSMT805 model

4.3 Parameter simulation

Conventional low-light imaging technology involves the transmission or reflection of visible light through the sample. Subsequently, the light passes through one or more lenses, resulting in the acquisition of a magnified image of a minuscule sample. Diffraction is a phenomenon in which light waves deviate from their original straight path and travel in a non-linear manner when they strike barriers or apertures during the propagation process. The user is advised to visually see the contrasting light and dark regions that manifest on the display. The distribution of light intensity can convey image information of things[8]. This study integrated the diffraction imaging theory of an LED light source as previously discussed by the research group[23]. A Matlab simulation program was developed. The wavelength of the light source was set to 435 nm, 475 nm, and 720 nm during simulation. The distance between the imaging screen and the micro-hole, as well as the size of the micro-hole, were adjusted until the desired diffraction image could be obtained. Based on the simulation results of the diffraction imaging system, it was determined that the CMOS image sensor was located 45 mm below the micro-hole, and the diameter of the micro-hole was 100 μm. The diffraction image obtained by simulation of the diffraction imaging system is shown in Figure 7. The diffraction image has clear diffraction fringes. The simulation parameters of the diffraction imaging system were appropriately set.

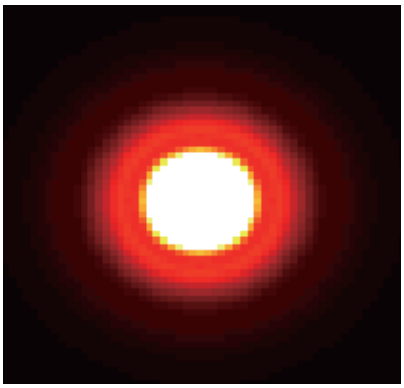

Figure 7 Simulation result for diffraction imaging system

5 Experimental results and analysis

5.1 Testing of diffraction imaging system for diseased spores

The device structure of the diffraction imaging system was designed using Solid Works software. The shell was printed using 3D printing technology. To mitigate the influence of external light, the 3D printing material was selected to possess a black coloration. The light source was powered by a charging bank, with the charging bank and the light source being connected through USB to TTL. The connection between the CMOS image sensor and the computer was established via a data cable. The software utilized for acquiring diffraction images of sick spores was Toup View. Figure 8 depicts the diffraction imaging system that has been constructed. The constructed diffraction imaging system successfully captures diffraction images of disease spores. Moreover, the diffraction images of the disease spores collected have clear diffraction fingerprints.

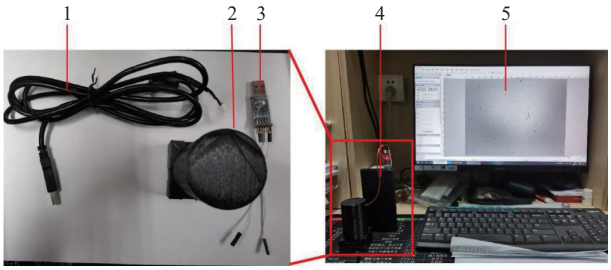

1. Data transmission line 2. Diffraction imaging device 3. USB to TTL 4. Powerbank 5. Computer

Figure 8 Photographs of the diffraction imaging system

5.2 Counting method of disease spores

This study used the angle spectrum reconstruction method to reconstruct the diffraction images of diseased spores. In order to obtain effective diffraction fingerprint image information, it is necessary to preprocess the spore diffraction image[23,24]. The specific steps were as follows: 1) The diffraction image was corrected by a two-dimensional gamma function; 2) The median filter was used to remove the noise signal from the diffraction image; 3) Diffraction images of diseased spores were reconstructed by angle spectrum reconstruction algorithm; 4) The diffraction images of diseased spores reconstructed by diagonal spectrum were processed, and the useless information was filtered by threshold segmentation; 5) The morphology operation was carried out, and the cavity filling and boundary smoothing was carried out; and 6) The morphological characteristics of disease spores were extracted, identified, and counted. The two characteristics of area and perimeter were selected in this study. The equations are as follows:

$$A = N \tag{1}$$

$$P = \sqrt{2}N_0 + N_e \tag{2}$$

where, A represents the region of the processed disease spore image; N represents the number of pixels in the processed disease spore image; P represents the circumference of the processed disease spore image; N_0 represents the diagonal pixel number of the processed disease spore image; N_e represents the number of horizontal or vertical pixels in the processed disease spore image.

The diffraction image processing and counting results of tomato gray mold spores obtained by the above method are shown in Figure 9.

5.3 Disease spore count results and analysis

The experimental results were analyzed statistically. The error of disease spore counting is defined as follows:

$$error = \frac{|n - n_0|}{n_0} \times 100\% \tag{3}$$

where, n represents the diffraction reconstruction counting results of diseased spores; n_0 represents the manual counting results of disease spores under a microscope.

The results are shown in Figure 10. The experimental error

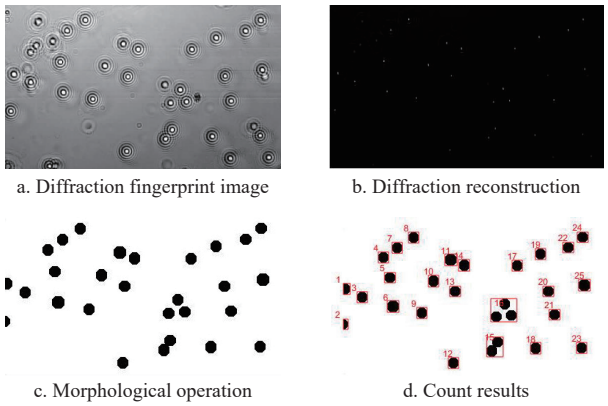

a. Diffraction fingerprint image b. Diffraction reconstruction

c. Morphological operation d. Count results

Figure 9 Tomato gray mold spore diffraction image processing and counting

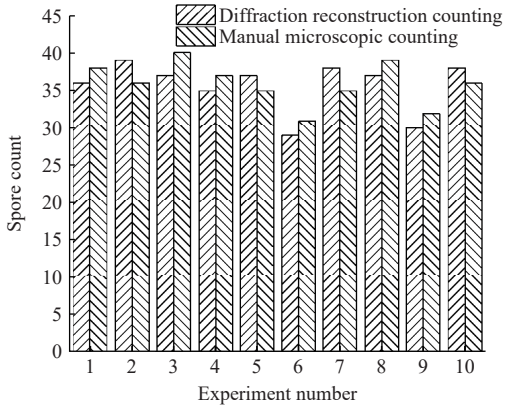

a. Comparison of counting results

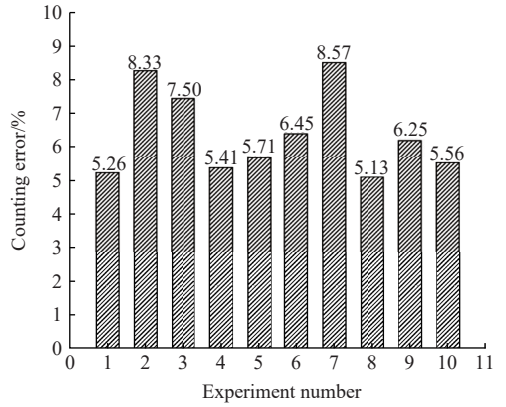

b. Counting error statistics

Figure 10 Comparison of counting results and error statistics between manual microscope count and diffraction image reconstruction

range was 5.13%-8.57% across the 10 group experiments. The average error of the experiments was 6.42%. There is no doubt that manual counting is more efficient than automatic counting based on processing diffraction images, but the overall accuracy of the latter is very acceptable. The error resulting during automatic counting may be due to the weak diffraction ring of some tomato gray mold spores, which are difficult to identify when using diffraction fingerprint images. Moreover, the spores vary in shape and size depending on the growth stages during which they were collected, leading to different patterns of diffraction fingerprints. The germination of tomato gray mold spores occurs exclusively when they infiltrate the tomato leaves and fruits, according to appropriate temperature and humidity conditions. To further demonstrate the practicality of quantifying tomato gray mold spores by diffraction fingerprint image processing, the Bland-Altman technique[25] was employed to evaluate the two counting approaches. All data points were inside the 95% confidence interval, indicating a high level of consistency. The findings of the study indicated that the enumeration of tomato gray mold spores using diffraction image processing yielded results consistent with those obtained by manual microscopic examination. The spores were counted by diffraction image processing.

6 Conclusions

The size, shape, protein, and nucleic acid of the tomato gray mold spores are different from other cells. The specific absorption spectrum information and diffraction imaging distance of tomato gray mold spores are likewise different from other cells. The existing lensless holographic imaging systems for cell detection cannot be directly applied to the detection of tomato gray mold spores. This study presents an approach for quantifying spore counts of tomato gray mold using diffraction imaging technology and image processing techniques. A device for acquiring diffraction images of tomato gray mold spores was constructed. Tomato gray mold spores were counted based on angular spectrum reconstruction and image processing. The average error of counting tomato gray mold spores based on diffraction reconstruction was 6.42%. This study can be used to aid in the detection of disease spores and provide technical means for early warning of greenhouse air-borne diseases.

Acknowledgements

This work was partially supported by the National Natural Science Foundation of China (Grant Nos. 32071905, 3217895, and 32201686), Priority Academic Program Development of Jiangsu Higher Education Institutions (Grant No. PAPD-2023-87), Agricultural Equipment Department of Jiangsu University (Grant No. NZXB20210106), National Key Research and Development Program for Young Scientists (Grant No. 2022YFD2000013), General Program of Basic Science (Natural Science) Research in Higher Education Institutions of Jiangsu Province (Grant No. 23KJB210004), and Natural Science Foundation of Jiangsu Province for Youth (Grant No. BK20240880).

[References]

[1] Mustapha A T, Zhou C S, Amanor-Atiemoh R, Ali T A A, Wahia H, Ma H L, et al. Efficacy of dual-frequency ultrasound and sanitizers washing treatments on quality retention of cherry tomato. Innovative Food Science & Emerging Technologies, 2020; 62: 102348.

[2] Shi Y, Yang Q Y, Zhao Q H, Dhanasekaran S, Ahima J, Zhang X Y, et al. *Aureobasidium pullulans* S-2 reduced the disease incidence of tomato by influencing the postharvest microbiome during storage. Postharvest Biology and Technology, 2022; 185: 111809.

[3] Zhang C, Li X Y, Yan H F, Ullah I Zuo Z Y, Li L L, et al. Effects of irrigation quantity and biochar on soil physical properties, growth characteristics, yield and quality of greenhouse tomato. Agricultural Water Management, 2020; 241: 106263.

[4] Mustapha A T, Zhou C S. Novel assisted/unassisted ultrasound treatment: Effect on respiration rate, ethylene production, enzymes activity, volatile composition, and odor of cherry tomato. LWT, 2021; 149: 111779.

[5] Zheng L N, Zhang J P, Wu X, Gu X H, Wang S L, Zhang H. A novel biocontrol strain *Pantoea jilinensis* D25 for effective biocontrol of tomato gray mold (causative agent *Botrytis cinerea*). Biological Control, 2021; 164: 104766.

[6] Raynaldo F A, Dhanasekaran S, Ngea G L N, Yang Q Y, Zhang X Y, Zhang H Y. Investigating the biocontrol potentiality of *Wickerhamomyces anomalus* against postharvest gray mold decay in cherry tomatoes. Scientia Horticulturae, 2021; 285: 110137.

[7] Sun G Z, Yang Q C, Zhang A C, Guo J, Liu X J, Wang Y, et al. Synergistic effect of the combined bio-fungicides epsilon-poly-L-lysine and chitooligosaccharide in controlling grey mould (*Botrytis cinerea*) in tomatoes. International Journal of Food Microbiology, 2018; 276: 46–53.

[8] Wang Y F, Mao H P, Zhang X D, Liu Y, Du X X. A rapid detection method for tomato gray mold spores in greenhouse based on microfluidic chip enrichment and lens-less diffraction image processing. Foods, 2021; 10(12): 3011.

[9] Wang J, Xia X M, Wang H Y, Li P P, Wang K Y. Inhibitory effect of lactoferrin against gray mould on tomato plants caused by *Botrytis cinerea* and possible mechanisms of action. International Journal of Food Microbiology, 2013; 161(3): 151–157.

[10] Sun Z B, Qi J H, Shen Y, Yang N, Liu S H, Wang A Y, et al. Collection, nucleic acid release, amplification, and visualization platform for rapid field detection of rice false smut. Lab on a Chip, 2023; 23(3): 542–552.

[11] Sireesha Y, Velazhahan R. Rapid and specific detection of *Peronosclerospora sorghi* in maize seeds by conventional and real-time PCR. European Journal of Plant Pathology, 2017; 150: 521–526.

[12] Lei Y, Yao Z F, He D J. Automatic detection and counting of urediniospores of *Puccinia striiformis* f. sp. tritici using spore traps and image processing. Scientific Reports, 2018; 8: 13647.

[13] Wang Y F, Zhang X D, Taha M F, Chen T H, Yang N, Zhang J R, et al. Detection method of fungal spores based on fingerprint characteristics of diffraction-polarization images. Journal of Fungi, 2023; 9(12): 1131.

[14] Luo Yi, Joung H-A, Esparza S, Rao J Y, Garner O, Ozcan A. Quantitative particle agglutination assay for point-of-care testing using mobile holographic imaging and deep learning. Lab on a Chip, 2021; 21(18): 3550–3558.

[15] Xiao W, Xin L, Cao R Y, Wu X T, Tian R, Che L P, et al. Sensing morphogenesis of bone cells under microfluidic shear stress by holographic microscopy and automatic aberration compensation with deep learning. Lab on a Chip, 2021; 21(7): 1385–1394.

[16] Prajapati E, Kumar S, Kumar S. Muscope: A miniature on-chip lensless microscope. Lab on a Chip, 2021; 21(22): 4357–4363.

[17] Xin L, Xiao X, Xiao W, Peng R, Wang H, Pan F. Screening for urothelial carcinoma cells in urine based on digital holographic flow cytometry through machine learning and deep learning methods. Lab on a Chip, 2024; 24(10): 2736–2746.

[18] Palacios-Ortega N, Del Socorro Hernandez-Montes M, Santoyo F M, Flores-Moreno M, de la Torre Ibarra M, Luis-Noriega D, et al. Simultaneous dual-wavelength digital holographic microscopy as a tool for the analysis of keratoacanthoma skin samples. Journal of Physics D: Applied Physics, 2024; 57(2): 025401.

[19] Fang W Q, Wang X Z, Han D L, Chen X G. Review of material parameter calibration method. Agriculture, 2022; 12(5): 706.

[20] Sun J, Hu S Q, Zhou X, Zhang L, Wu X D, Dai C X. Design and experiment of portable non-destructive tester for heavy metal cadmium content in vegetable leaves. Transactions of the CSAM, 2022; 53(2): 195–202, 220. (in Chinese)

[21] Chen Y Y, Cheng Q Q, Fang X M, Yu H H, Li D L. Principal component analysis and long short-term memory neural network for predicting dissolved oxygen in water for aquaculture. Transactions of the CSAE, 2018; 34(17): 183–191. (in Chinese)

[22] Wang Y F, Zhang X D, Yang N, Ma G X, Du X Y, Mao H P. Separation-enrichment method for airborne disease spores based on microfluidic chip. Int J Agric & Biol Eng, 2021; 14(5): 199–205.

[23] Yang N, Chen C Y, Li G X, Wang A Y, Zhang R B, Tang J. Micro detection device for fungal spores of crops based on diffraction reconstruction. Transactions of the CSAM, 2019; 50(4): 42–48. (in Chinese)

[24] Woyzichovski J, Shchepin O, Dagamac N H, Schnittler M. A workflow for low-cost automated image analysis of myxomycete spore numbers, size and shape. PeerJ, 2021; 9: e12471.

[25] Ashley-Martin J, Gaudreau É, Dumas P, Liang C L, Logvin A, Bélanger P, et al. Direct LC-MS/MS and indirect GC-MS/MS methods for measuring urinary bisphenol A concentrations are comparable. Environment International, 2021; 157: 106874.